Biophysical Journal, Volume *110*

Supplemental Information

Cell Surface Mechanochemistry and the Determinants of Bleb Formation, Healing, and Travel Velocity

Kathryn Manakova, Huaming Yan, John Lowengrub, and Jun Allard

Cell surface mechanochemistry and the determinants of bleb formation, healing and travel velocity

Kathryn Manakova[†], Huaming Yan[†], John Lowengrub[†]
and Jun Allard[†‡*]

[†]Department of Mathematics, Center for Complex Biological Systems, [‡]Department of Physics and Astronomy, University of California, Irvine, [*]Corresponding author

Contents

1 Summary of experimental predictions

The model makes several testable predictions throughout the Results section. For convenience, we tabulate these predictions here. Note that these predictions presume that the cell is exhibiting blebs before the perturbation.

Table S1: Model predictions for experimental perturbations.

Experimental perturbation	Parameter	Prediction
Increasing hydrostatic pressure	$P \uparrow$	Larger blebs
Increasing molecular size of adhesion molecules	$D \uparrow$	Abolish blebbing
Decreasing molecular size of adhesion molecules	$D \downarrow$	Slower bleb healing
Increasing myosin contractility	$M \uparrow$	Abolish blebbing
Decreasing myosin contractility	$M \downarrow$	Slower bleb healing
Increasing membrane tension	$\gamma_M \uparrow$	Faster bleb travel
Increasing abundance of adhesions	$k_{\text{on}} \uparrow$	Slower bleb travel

2 Details of geometry of cortical and cytoplasmic actin

In 3D, the cell surface and cortex are curved, discontinuous two-dimensional manifolds and the cytoplasm is a 3D field. In full generality, the cortex and cytoplasmic actin network have a density at each point in space. We assume that actin-myosin contractility is isotropic and generates local stress proportional to the local density of cortical actin c. This stress therefore has two components: a tangential component due to connection with nearby cortex

$$\sigma_t = \sigma_M w_c c \nabla y_C, \tag{S1}$$

and a normal stress due to connection with the cytoplasmic actin network

$$\sigma_n = \sigma_M c y_C. \tag{S2}$$

We find that the normal contractile force is necessary for asymetric bleb healing, as occurs during bleb travel. This necessity can be understood from Fig. 1A: In the absence of cytoplasmic actin, the tangential stress pulls the membrane tangentially, but there is no force driving the cortex into the place of the cell. Our goal is to understand in 3D. To this end, we find it informative to study simplified 2D systems and 1D systems as an analytical tool. The 2D model is equivalent to either the geometries shown in Supplemental Fig. 1C

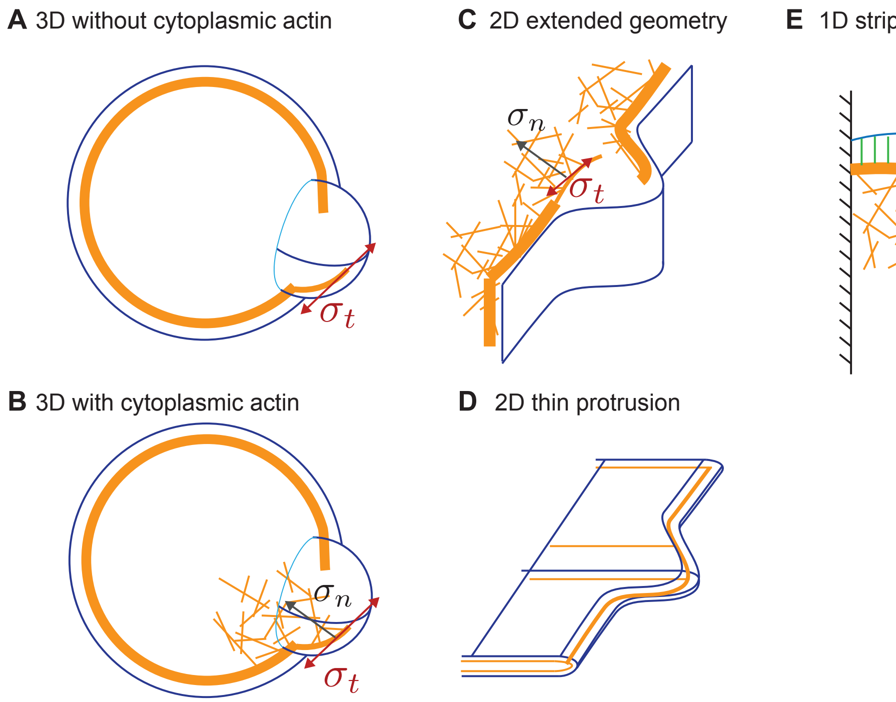

Figure S1: Approximations of cortex and cytoplasmic actin geometry in 3D. (A-B) Bleb geometry in 3D including only tangential cortical contractility (A), and both tangential and normal contractility (B). (C-D) Representation of 2D model. (E) Hypothetical 1D "non-spatial" model corresponding to ODE system used in Main Text.

or D. The 1D model, which we refer to as the ODE model in the Main Text, corresponds to the geometry shown in Supplemental Fig. 1E.

Table S2: Estimates of parameters used in non-dimensionalization.

Model parameter	Estimated value	Source
r	$0.1/s$	(11)
k_{on}	$100/\,\mu\text{m}^2 \cdot \text{s}$	(21)
k_{off}	$1/s$	(11)
k_A	$10\,\text{pN}/\mu m$	(21)
σ_M	$0.1\text{Pa}/\,\mu\text{m}^2$	(21)
$\hat{\Pi}$	$100\text{Pa}/\,\mu\text{m}$	(21)
y_M^0	$3\,\mu\text{m}$	(8)
γ_M	$100\,\text{pN}/\,\mu\text{m}$	(45)

3 Parameter estimation

Using these estimates, the correspondence between dimensional and non-dimensional parameters are given by

$$x = \chi \cdot 0.2\,\mu\text{m} \tag{S3}$$

$$t = \tau \cdot 10s \tag{S4}$$

$$a = A \cdot 100/\mu m^2 \tag{S5}$$

$$y_M = Y_M \cdot 3\,\mu\text{m} \tag{S6}$$

$$y_C = Y_C \cdot 3\,\mu\text{m}. \tag{S7}$$

Note that model parameters not included in Table S2 do not impact the non-dimensionalization.

4 Model variants

4.1 Bending

The inclusion of higher-order derivatives in the mechanical energy transform the system into a higher-order boundary value problem. For example, the bending energy term transforms the membrane shape equation to a fourth-order equation. We simulate the base model with the addition of bending terms $\beta > 0$, shown in Fig. S2. We find that the excitable parameter regime and traveling parameter regimes are unchanged. For $\beta = 100$, the velocity of travel is increased by approximately two-fold and healing is delayed compared to no bending.

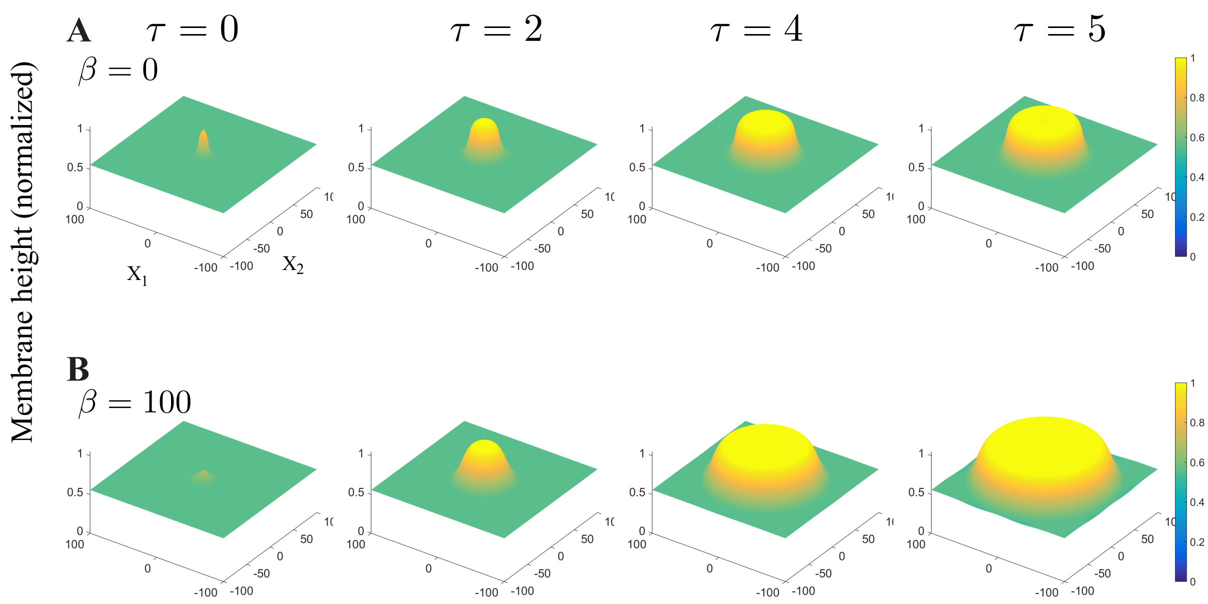

Figure S2: Influence of membrane bending rigidity. (A) Traveling bleb on a uniform surface with no bending energy $\beta = 0$. (B) Traveling bleb with large bending rigidity $\beta = 100$. The bleb velocity is increased by approximately two-fold and healing is delayed (but eventually occurs, not shown).

5 Details of numerical method

5.1 Base model

The base model, Eqs. 10-13, comprise a two-dimensional boundary value problem of elliptic type at each instant in time, coupled to two first-order (in time) partial differential equations. To solve the base model, we discretize space into a uniform grid of width $\Delta\chi = 0.1$ and time step size $\Delta t = 0.01$. We use a standard five-point stencil finite difference method in space and forward-Euler in time.

5.2 Non-uniform tension

The inclusion of non-uniform tension changes the boundary value problem to a non-uniform elliptic equation. The equations takes the form

$$P = f(\chi_1, \chi_2)Y_M(\chi_1, \chi_2) - \nabla \cdot (\Gamma(\chi_1, \chi_2)\nabla Y_M(\chi_1, \chi_2)) \tag{S8}$$

where f and Γ are spatially varying. We use a uniform grid in space and set $\Delta\chi = 0.1$. The functions f, Y_M and Γ all live at cell edges ($f|_{i,j} = f(i\Delta\chi,\ j\Delta\chi),\quad i = 1, 2, ..., 2000$) and we impose periodic boundary conditions. The parameter functions f and Γ must be interpolated to the edges, which we do by uniform averaging. The resulting discretization stencil is given by

$$\begin{aligned} P = &\left(f|_{i,j} + \frac{1}{2\Delta x^2} \left(\gamma|_{i+1,j} + \gamma|_{i-1,j} + \gamma|_{i,j+1} + \gamma|_{i,j-1} + 4\gamma|_{i,j} \right) \right) \mathbf{Y_M}|_{\mathbf{i,j}} \\ &- \frac{1}{2\Delta x^2} \left((\gamma|_{i+1,j} + \gamma|_{i,j}) \mathbf{Y_M}|_{\mathbf{i+1,j}} + (\gamma|_{\mathbf{i,j}} + \gamma|_{\mathbf{i,j-1}}) \mathbf{Y_M}|_{\mathbf{i-1,j}} \right) \\ &\quad - \frac{1}{2\Delta x^2} \left((\gamma|_{i,j} + \gamma|_{i,j+1}) \mathbf{Y_M}|_{\mathbf{i,j+1}} + (\gamma|_{\mathbf{i,j}} + \gamma|_{\mathbf{i,j-1}}) \mathbf{Y_M}|_{\mathbf{i,j-1}} \right) \end{aligned}$$

Since this equation remains linear, it can be written into a sparse matrix and solved as a linear system.

5.3 Higher-order models including bending forces

Adding higher order terms, including bending forces, transforms the boundary value problem into a higher-order boundary value problem. The bending term, in particular, introduces a fourth-order bilaplacian operator. This significantly increases the computational cost of solving the equations, therefore we use a more sophisticated solver described here. We solve the following equations:

$$\frac{\partial C}{\partial t} = \alpha A - C \tag{S9}$$

$$\epsilon \frac{\partial A}{\partial t} = \frac{C}{1 + C} \exp\left(- \left(\frac{1}{D} \frac{MC}{A + MC} Y_m \right) \right) - A \exp\left(\frac{1}{F_0} \frac{MC}{A + MC} Y_m \right) \tag{S10}$$

$$P = hY_m - \nabla \cdot (\Gamma \nabla Y_m) + B\nabla^4 Y_m \tag{S11}$$

$$h = \frac{AMC}{A + MC} + P, \tag{S12}$$

where $\alpha = 57, \epsilon = 0.1, D = 0.15, F_0 = 1, M = 0.007$ and $P = 0.1$. The nondimensional bending modulus is $B \equiv \beta/\gamma x_c^3$. In non-uniform tension models, $B = 0$ and the non-uniform tension term $\Gamma = 1 + \theta C$ where $\theta = 0.1$ or $\theta = 0.2$. For bending models, $\Gamma = 1$ and $B \in \{10^{-2}, 10^{-1}, 1, 10^1, 10^2\}$.

All variables satisfy periodic conditions at all boundaries. The initial condition for Y_m and C is their steady state value $Y_m^{ss} = 0.5582$ and $C^{ss} = 15.8236$. A is also set to steady state $A^{ss} = 0.2776$ except that $A = 0$ where $r = \sqrt{x^2 + y^2} < 5$.

The system is solved in a square computational domain $[-200, 200]^2$. The domain is initialized to a 64×64 mesh with a maximum of 5 refinement levels. At the finest level, grid length is $400/(64 \times 2^5) \approx 0.2$. The time step is 10^{-2}.

We use the implicit second order Crank-Nicholson scheme for time discretization in Eqs. (S9) and (S10). Spatial derivatives are discretized using central difference approximations. Eq. (S11) is reformulated as a system of two second order equations. Block structured Cartesian refinement is used to efficiently resolve the multiple spatial scales. In particular, the mesh is refined in regions with large spatial gradients of Y_m (typically around the bleb). The equations at implicit time level are solved by the adaptive nonlinear multigrid method developed in (46).

6 Description of Supplemental Movies

- **Supplemental Movie 1**. We simulate the 2D model with boundary conditions at the top and bottom (12-o-clock and 6-o-clock). Corresponds to parameters in Fig. 4A
- **Supplemental Movie 2**. Stationary bleb in 3D. Corresponds in Fig 2B.
- **Supplemental Movie 3**. Traveling bleb in 3D on a uniform surface. Travel is unrestricted and the excitation spreads in all directions.
- **Supplemental Movie 4**. Traveling bleb with surface heterogeneity. Corresponds to Fig. 4B.
- **Supplemental Movie 5**. Traveling bleb with global pressure. Corresponds to Fig. 6A.

References

[1] Allard, J. F., O. Dushek, D. Coombs, and P. A. Van Der Merwe, 2012. Mechanical Modulation of Receptor-Ligand Interactions at Cell-Cell Interfaces. *Biophys J* 102:1265–1273.

[2] Zhu, C., 2013. Mechanochemitry: A Molecular Biomechanics View of Mechanosensing. *Annals Biomed Eng* 42:388–404.

[3] Allard, J., and A. Mogilner, 2012. Traveling waves in actin dynamics and cell motility. *Curr Op Cell Biol* 25:1–9.

[4] Rangamani, P., A. Benjamini, A. Agrawal, B. Smit, D. J. Steigmann, and G. Oster, 2013. Small scale membrane mechanics. *Biomech Modeling Mechanobiology* .

[5] Liu, J., Y. Sun, G. F. Oster, and D. G. Drubin, 2010. Mechanochemical crosstalk during endocytic vesicle formation. *Curr Op Cell Biol* 22:36–43.

[6] Tinevez, J.-Y., U. Schulze, G. Salbreux, J. Roensch, J.-F. Joanny, and E. Paluch, 2009. Role of cortical tension in bleb growth. *Proc Natl Acad Sci USA* 106:18581–18586.

[7] Peleg, B., A. Disanza, G. Scita, and N. Gov, 2011. Propagating Cell-Membrane Waves Driven by Curved Activators of Actin Polymerization. *PLoS ONE* 6:e18635.

[8] Clark, A. G., K. Dierkes, and E. K. Paluch, 2013. Monitoring Actin Cortex Thickness in Live Cells. *Biophys J* 105:570–580.

[9] Salbreux, G., J. Prost, and J. F. Joanny, 2009. Hydrodynamics of Cellular Cortical Flows and the Formation of Contractile Rings. *Phys Rev Lett* 103:058102.

[10] Hannezo, E., B. Dong, P. Recho, J.-F. Joanny, and S. Hayashi, 2015. Cortical instability drives periodic supracellular actin pattern formation in epithelial tubes. *Proc Natl Acad Sci USA* 112:8620–8625.

[11] Fritzsche, M., R. Thorogate, and G. Charras, 2014. Quantitative Analysis of Ezrin Turnover Dynamics in the Actin Cortex. *Biophys J* 106:343–353.

[12] Strychalski, W., and R. D. Guy, 2013. A computational model of bleb formation. *Math Med Biol* 30:115–130.

[13] Charras, G. T., T. J. Mitchison, and L. Mahadevan, 2009. Animal cell hydraulics. *J Cell Sci* 122:3233–3241.

[14] Clark, A. G., O. Wartlick, G. Salbreux, and E. K. Paluch, 2014. Stresses at the Cell Surface during Animal Cell Review Morphogenesis. *Curr Biol* 24:R484–R494.

[15] Fogelson, B., and A. Mogilner, 2014. Computational Estimates of Membrane Flow and Tension Gradient in Motile Cells. *PLoS ONE* 9:e84524.

[16] Yip, A.Km Chiam, K.-H. and P. Matsudaira, 2015. Traction stress analysis and modeling reveal that amoeboid migration in confined spaces is accompanied by expansive forces and requires the structural integrity of the membrane-cortex interactions. *Integrative Biology* 7:1196–1211.

[17] Weiner, O. D., W. A. Marganski, L. F. Wu, S. J. Altschuler, and M. W. Kirschner, 2007. An Actin-Based Wave Generator Organizes Cell Motility. *PLoS Biology* 5:e221.

[18] Leijnse, N., L. B. Oddershede, and P. M. Bendix, 2015. An updated look at actin dynamics in filopodia. *Cytoskeleton* 72:71–79.

[19] Wollman, R., and T. Meyer, 2012. Coordinated oscillations in cortical actin and Ca2+ correlate with cycles of vesicle secretion. *Nat Cell Biol* 14:1261–1269.

[20] Charras, G. T., 2008. A short history of blebbing. *J Microscopy* 231:466–478.

[21] Charras, G. T., Coughlin, M., Mitchison, T. and Mahadevan, L., 2008. Life and times of a cellular bleb. *Biophys J* 94:1836–1853.

[22] Paluch, E. K., and E. Raz, 2013. The role and regulation of blebs in cell migration. *Curr Op Cell Biol* 25:582–590.

[23] Danuser, G., J. Allard, and A. Mogilner, 2012. Mathematical Modeling of Eukaryotic Cell Migration: Insights Beyond Experiments. *Annu Rev Cell Dev Biol* 18.1-18.28.

[24] Fujinami, N., and T. Kageyama, 1975. Circus movement in dissociated embryonic cells of a teleost, Oryzias latipes. *J Cell Sci* 19:169–182.

[25] Olson, E. C., 1996. Onset of electrical excitability during a period of circus plasma membrane movements in differentiating Xenopus neurons. *J Neurosci* 16:5117–5129.

[26] Lim, F. Y., K.-H. Chiam, and L. Mahadevan, 2012. The size, shape, and dynamics of cellular blebs. *Europhys Lett* 100:28004.

[27] Logue, J. S., A. X. Cartagena-Rivera, M. A. Baird, M. W. Davidson, R. S. Chadwick, and C. M. Waterman, 2015. Erk regulation of actin capping and bundling by Eps8 promotes cortex tension and leader bleb-based migration. *eLife* 4.

[28] Charras, G., and E. Paluch, 2008. Blebs lead the way: how to migrate without lamellipodia. *Nat Rev Mol Cell Biol* 9:730–736.

[29] Friedl, P., and K. Wolf, 2003. Tumour-cell invasion and migration: diversity and escape mechanisms. *Nat Rev Cancer* 3:362–374.

[30] Sedzinski, J., M. Biro, A. Oswald, J.-Y. Tinevez, G. Salbreux, and E. Paluch, 2011. Polar actomyosin contractility destabilizes the position of the cytokinetic furrow. *Nature* 476:462–466.

[31] Baum, D. A., and B. Baum, 2014. An inside-out origin for the eukaryotic cell. *BMC Biology* 12:76.

[32] Ryan, G. L., N. Watanabe, and D. Vavylonis, 2012. A review of models of fluctuating protrusion and retraction patterns at the leading edge of motile cells. *Cytoskeleton* 69:195–206.

[33] Kapustina, M., T. C. Elston, and K. Jacobson, 2013. Compression and dilation of the membrane-cortex layer generates rapid changes in cell shape. *J Cell Biol* 200:95–108.

[34] Strychalski, W., C. A. Copos, O. L. Lewis, and R. D. Guy, 2015. A poroelastic immersed boundary method with applications to cell biology. *J Comp Phys* 282:77–97.

[35] Young, J., and S. Mitran, 2010. A numerical model of cellular blebbing: A volume-conserving, fluid–structure interaction model of the entire cell. *J Biomech* 43:210–220.

[36] Alert, R., J. Casademunt, J. Brugués, and P. Sens, 2015. Model for Probing Membrane-Cortex Adhesion by Micropipette Aspiration and Fluctuation Spectroscopy. *Biophys J* 108:1878–1886.

[37] Woolley, T. E., E. A. Gaffney, J. M. Oliver, R. E. Baker, S. L. Waters, and A. Goriely, 2013. Cellular blebs: pressure-driven, axisymmetric, membrane protrusions. *Biomech Modelling Mechanobiol* 13:463–476.

[38] Woolley, T. E., E. A. Gaffney, S. L. Waters, J. M. Oliver, R. E. Baker, and A. Goriely, 2014. Three mechanical models for blebbing and multi-blebbing. *IMA J Applied Math* 79:636–660.

[39] Woolley, T. E., E. A. Gaffney, and A. Goriely, 2015. Membrane shrinkage and cortex remodelling are predicted to work in harmony to retract blebs. *R Soc Open Science* 2:150184–15.

[40] Bovellan, M., Y. Romeo, M. Biro, A. Boden, P. Chugh, A. Yonis, M. Vaghela, M. Fritzsche, D. Moulding, R. Thorogate, A. Jégou, A. J. Thrasher, G. Romet-Lemonne, P. P. Roux, E. K. Paluch, and G. Charras, 2014. Cellular Control of Cortical Actin Nucleation. *Curr Biol* 24:1628–1635.

[41] Paszek, M. J., C. C. DuFort, O. Rossier, R. Bainer, J. K. Mouw, K. Godula, J. E. Hudak, J. N. Lakins, A. C. Wijekoon, L. Cassereau, M. G. Rubashkin, M. J. Magbanua, K. S. Thorn, M. W. Davidson, H. S. Rugo, J. W. Park, D. A. Hammer, G. Giannone, C. R. Bertozzi, and V. M. Weaver, 2015. The cancer glycocalyx mechanically primes integrin-mediated growth and survival. *Nature* 511:319–325.

[42] Helfrich, W., 1973. Elastic properties of lipid bilayers: theory and possible experiments. Zeitschrift für Naturforschung. Teil C: Biochemie.

[43] Charras, G. T., J. C. Yarrow, M. A. Horton, L. Mahadevan, and T. J. Mitchison, 2005. Non-equilibration of hydrostatic pressure in blebbing cells. *Nature* 435:365–369.

[44] Taloni, A., E. Kardash, O. Salman,L. Truskinovsky,4 S. Zapperi, and C. La Porta, 2015. Volume Changes During Active Shape Fluctuations in Cells. *Phys Rev Lett* 114:208101.

[45] Peukes, J., and T. Betz, 2014. Direct Measurement of the Cortical Tension during the Growth of Membrane Blebs. *Biophys J* 107:1810–1820.

[46] Wise, S. M., Kim, J. Lowengrub, J. S., 2007 Solving the regularized, strongly anisotropic Cahn-Hilliard equation by an adaptive nonlinear multigrid method. *J Comp Phys*, 226:414-416.

[47] Edelstein-Keshet, L., 1988. Mathematical Models in Biology .

[48] Idema, T., T. Idema, J. O. Dubuis, J. O. Dubuis, L. Kang, L. Kang, M. L. Manning, M. L. Manning, P. C. Nelson, P. C. Nelson, T. C. Lubensky, and A. J. Liu, 2013. The syncytial Drosophila embryo as a mechanically excitable medium. *PLoS ONE* .

[49] Ryan, G. L., H. M. Petroccia, N. Watanabe, and D. Vavylonis, 2012. Excitable Actin Dynamics in Lamellipodial Protrusion and Retraction. *Biophys J* 102:1493–1502.

[50] Bement, W. M., M. Leda, A. M. Moe, A. M. Kita, M. E. Larson, A. E. Golding, C. Pfeuti, K.-C. Su, A. L. Miller, A. B. Goryachev, and others, 2015. Activator-inhibitor coupling between Rho signalling and actin assembly makes the cell cortex an excitable medium. *Nat Cell Biol* .

[51] Britton, N. F., 1982. Threshold phenomena and solitary traveling waves in a class of reaction-diffusion systems. *SIAM J Applied Math* .

[52] Mori, Y., A. Jilkine, and L. Edelstein-Keshet, 2008. Wave-pinning and cell polarity from a bistable reaction-diffusion system. *Biophys J* 94:3684–3697.

[53] Strychalski, W., and R. D. Guy, 2016. Intracellular Pressure Dynamics in Blebbing Cells. *Biophys J.* In press.

[54] Huang, C.-H., M. Tang, C. Shi, P. A. Iglesias, and P. N. Devreotes, 2013. An excitable signal integrator couples to an idling cytoskeletal oscillator to drive cell migration. *Nat Cell Biol* 15:1307–1316.

[55] Xiong, Y., C.-H. Huang, P. A. Iglesias, and P. N. Devreotes, 2010. Cells navigate with a local-excitation, global-inhibition-biased excitable network. *Proc Natl Acad Sci USA* 107:17079–17086.

[56] FitzHugh, R., 1961. Impulses and Physiological States in Theoretical Models of Nerve Membrane. *Biophys J* 1:445–466.

[57] Lee, J., A. Ishihara, J. A. Theriot, and K. Jacobson, 1993. Principles of locomotion for simple-shaped cells. *Nature* 362:167–171.

[58] Luo, W., C. Yu, Z. Lieu, J. Allard, A. Mogilner, M. Sheetz, A. Bershadsky, 2013. Analysis of the local organization and dynamics of cellular actin networks. *J Cell Biol* 202:1057–1073.

[59] Thon, J. N., H. Macleod, A. J. Begonja, J. Zhu, K.-C. Lee, A. Mogilner, J. H. Hartwig, and J. E. Italiano, 2012. Microtubule and cortical forces determine platelet size during vascular platelet production. *Nat Comm* 3:852–9.

[60] Dobrowsky, T. M., B. R. Daniels, R. F. Siliciano, S. X. Sun, and D. Wirtz, 2010. Organization of Cellular Receptors into a Nanoscale Junction during HIV-1 Adhesion. *PLoS Comp Biol* 6:e1000855.

[61] Qi, S., M. Krogsgaard, M. M. Davis, and A. K. Chakraborty, 2006. Molecular flexibility can influence the stimulatory ability of receptor-ligand interactions at cell-cell junctions. *Proc Natl Acad Sci USA* 103:4416–4421.

[62] Murray, J. D., 1989. Mathematical Biology. Springer

[63] Carlson, A., and L. Mahadevan, 2016. Elastohydrodynamics and kinetics of protein patterning in the immunological synapse. *PLoS Comp Biol* 11:e1004481.

[64] Biro, M., Y. Romeo, S. Kroschwald, M. Bovellan, A. Boden, J. Tcherkezian, P. P. Roux, G. Charras, and E. K. Paluch, 2013. Cell cortex composition and homeostasis resolved by integrating proteomics and quantitative imaging. *Cytoskeleton* 70:741–754.